Superconductivity induced by interfacial coupling to magnons

Niklas Rohling, Eirik Løhaugen Fjærbu, and Arne Brataas
Center for Quantum Spintronics, Department of Physics, Norwegian University of Science and Technology, NO-7491 Trondheim, Norway

(Received 13 July 2017; published 1 March 2018)

We consider a thin normal metal sandwiched between two ferromagnetic insulators. At the interfaces, the exchange coupling causes electrons within the metal to interact with magnons in the insulators. This electron-magnon interaction induces electron-electron interactions, which in turn can result in p-wave superconductivity. We solve the gap equation numerically and estimate the critical temperature. In yttrium iron garnet (YIG)-Au-YIG trilayers, superconductivity sets in at temperatures somewhere in the interval between 1 and 10 K. EuO-Au-EuO trilayers require a lower temperature, in the range from 0.01 to 1 K.

DOI: 10.1103/PhysRevB.97.115401

I. INTRODUCTION

The interactions between electrons in a conductor and ordered spins across interfaces are of central importance in spintronics [1,2]. Here, we focus on the case in which the magnetically ordered system is a ferromagnetic insulator (FI). The interaction at an FI-normal metal (NM) interface can be described in terms of an exchange coupling [3–6]. In the static regime, this coupling induces effective Zeeman fields near the boundary [7–10]. The magnetization dynamics caused by the coupling can be described in terms of the spin-mixing conductance [4–6]. Such dynamics can include spin pumping from the FI into the NM [11,12] and its reciprocal effect, spin-transfer torques [5,13]. These spin-transfer torques enable electrical control of the magnetization in FIs [14].

One important characteristic of FIs is that the Gilbert damping is typically small. This leads to low-dissipation magnetization dynamics [15], which in turn facilitates coherent magnon dynamics and the long-range transport of spin signals [5,13]. These phenomena should also enable other uses of the quantum nature of the magnons.

Here, we study an effect that is also governed by the electron-magnon interactions at FI-NM interfaces but is qualitatively different from spin pumping and spin-transfer torques. We explore how the magnons in FIs can mediate superconductivity in a metal. The exchange coupling at the interfaces between the FIs and the NM induces Cooper pairing. In this scenario, the electrons and the magnons mediating the pairing reside in two different materials. This opens up a wide range of possibilities for tuning the superconducting properties of the system by combining layers with the desired characteristics. The electron and magnon dispersions within the layers as well as the electron-magnon coupling between the layers influence the pairing mechanism. Consequently, the superconducting gap can also be tuned by modifying the layer thickness, interface quality, and external fields.

Since the interactions occur at the interfaces, the consequences of the coupling are most pronounced when the NM layer is thin. We therefore consider atomically thin FI and NM layers. This also reduces the complexity of the calculations. For thicker layers, multiple modes exist along the direction transverse to the interface (x), with different effective coupling strengths. We expect a qualitatively similar, but somewhat weaker, effect for thicker layers.

Paramagnonic [16] or magnonic [17] coupling may explain experimental observations of superconductivity coexisting with ferromagnetism in bulk materials [18–20]. Paramagnons [16,21] and magnons [17,22] are predicted to mediate triplet p-wave pairing with equal and antiparallel spins, respectively. Reference [22] describes a model for a bulk ferrimagnetic spinel, where magnons residing on one sublattice mediate a superconductive pairing of electrons that reside on the other sublattice. In that model, an external magnetic field compensates the exchange-induced Zeeman splitting. By contrast, we consider interface-induced superconductivity in a layered system consisting of three thin films.

High-quality thin films offer new possibilities for superconductivity [23]. Consequently, the emergence of superconductivity at interfaces has recently received considerable attention [23–31]. Theoretical studies have been conducted on interface-induced superconductivity mediated by phonons [27–29], excitons [32], and polarizable localized excitations [31,33].

A model of interface-induced magnon-mediated d-wave pairing has been proposed to explain the observed superconductivity in Bi/Ni bilayers [34]. A p-wave pairing of electrons with equal momentum—so-called Amperean pairing—has been predicted to occur in a similar system [35]. Importantly, the electrons that form pairs in these models reside in a spin-momentum-locked surface conduction band.

By contrast, we consider a spin-degenerate conduction band in an FI-NM-FI trilayer. We find interfacially mediated p-wave superconductivity with antiparallel spins and momenta. These pairing symmetries are distinct from those of the two-dimensional (2D) systems mentioned above.

II. MODEL

We assume that the equilibrium magnetization of the left (right) FI is along the $\hat{z}$ ($-\hat{z}$) direction; see Fig. 1. We consider matching square lattices, with lattice constant a, in all three monolayers. The interfacial plane consists of N sites with periodic boundary conditions. The Hamiltonian is

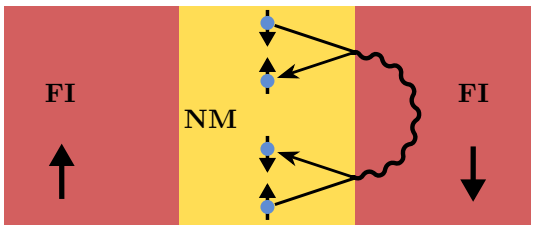

FIG. 1. A trilayer formed of a normal metal between two ferromagnetic insulators. The magnetizations are antiparallel. At the interfaces, conduction electrons couple to magnons. This results in effective electron-electron interactions in the metal.

$H = H_{\rm FI}^A + H_{\rm FI}^B + H_{\rm NM} + H_{\rm int}$, where we use A (B) to denote the left (right) FI.

The Heisenberg Hamiltonian

$$H_{\rm FI}^A = -\frac{J}{\hbar^2}\sum_i \sum_{j\in {\rm NN}(i)} \mathbf{S}_i^A \cdot \mathbf{S}_j^A \tag{1}$$

describes the left FI. Here, i is an in-plane site, NN(i) is the set of its nearest neighbors, J is the exchange interaction, and $\mathbf{S}_i^A$ is the localized spin at site i. The expression for $H_{\rm FI}^B$ is similar.

For the time being, we assume that the conduction electron eigenstates in the NM are plane waves of the form $c_{\mathbf{q},\sigma} = \sum_j \exp(i\mathbf{r}_j\cdot\mathbf{q})c_{j\sigma}/\sqrt{N}$. Here, $c_{j\sigma}^{(\dagger)}$ annihilates (creates) a conduction electron with spin σ at site j in the NM, and $\mathbf{q}$ is the wave vector. For now, the NM Hamiltonian is $H_{\rm NM} = \sum_{\mathbf{q}}\sum_\sigma E_{\mathbf{q}} c_{\mathbf{q}\sigma}^\dagger c_{\mathbf{q}\sigma}$ with the quadratic dispersion $E_{\mathbf{q}} = \hbar^2\mathbf{q}^2/(2m)$. Here, m is the effective electron mass. Below, when estimating the coupling J_I at yttrium iron garnet (YIG)-Au interfaces, we consider another Hamiltonian with different eigenstates and a different dispersion.

We model the coupling between the conduction electrons and the localized spins as an exchange interaction [4,5,36,37],

$$H_{\rm int} = -2\frac{J_I}{\hbar}\sum_{\sigma\sigma'}\sum_j\sum_{L=A,B} c_{j\sigma}^\dagger \boldsymbol{\sigma}_{\sigma\sigma'} c_{j\sigma'}\cdot \mathbf{S}_j^L, \tag{2}$$

where $\boldsymbol{\sigma} = (\sigma_x,\sigma_y,\sigma_z)$ is a vector of Pauli matrices.

After a Holstein-Primakoff transformation, we expand the Hamiltonian of Eq. (1) up to second order in the bosonic operators. We represent $\mathbf{S}_j^A$ by $S_{jx}^A + iS_{jy}^A = \hbar\sqrt{2s}a_j$, $S_{jx}^A - iS_{jy}^A = \hbar\sqrt{2s}a_j^\dagger$, and $S_{jz}^A = \hbar(s - a_j^\dagger a_j)$, where s is the spin quantum number of the localized spins and $a_j^{(\dagger)}$ is a bosonic annihilation (creation) operator at site j. The magnons in layer A, with the form $a_{\mathbf{k}} = \sum_{j\in A}\exp(i\mathbf{r}_j\cdot\mathbf{k})a_j/\sqrt{N}$, are eigenstates of the resulting Hamiltonian. Analogously, magnons in layer B are denoted $b_{\mathbf{k}}$. The magnon dispersion is

$$\varepsilon_{\mathbf{k}} = 4sJ[2 - \cos(k_y a) - \cos(k_z a)]. \tag{3}$$

Disregarding second-order terms in the bosonic operators from the interfacial coupling yields

$$H = \sum_{\mathbf{k}}\varepsilon_{\mathbf{k}}(a_{\mathbf{k}}^\dagger a_{\mathbf{k}} + b_{\mathbf{k}}^\dagger b_{\mathbf{k}}) + \sum_{\mathbf{q}\sigma} E_{\mathbf{q}} c_{\mathbf{q}\sigma}^\dagger c_{\mathbf{q}\sigma} + \sum_{\mathbf{kq}} V(a_{\mathbf{k}} c_{\mathbf{q}+\mathbf{k},\downarrow}^\dagger c_{\mathbf{q}\uparrow} + b_{\mathbf{k}} c_{\mathbf{q}+\mathbf{k},\uparrow}^\dagger c_{\mathbf{q}\downarrow} + {\rm H.c.}), \tag{4}$$

where $V = -2J_I\sqrt{s}/\sqrt{2N}$ is the coupling strength between the electrons in the NM and the magnons in the FI layers.

There is no induced Zeeman field in the NM since the magnetizations in the FIs are antiparallel. Even if the NM contained more than one atomic layer, spin-up and spin-down electrons would still be degenerate, as the system is invariant under the combined operation of time reversal and spatial inversion.

III. THE SUPERCONDUCTING GAP

Analogously to phonon-mediated coupling in conventional superconductors, the magnons mediate effective interactions between the electrons. For electron pairs with opposite momenta, we obtain

$$H_{\rm pair} = \sum_{\mathbf{kk}'} V_{\mathbf{kk}'} c_{\mathbf{k}\downarrow}^\dagger c_{-\mathbf{k}\uparrow}^\dagger c_{-\mathbf{k}'\uparrow} c_{\mathbf{k}'\downarrow}, \tag{5}$$

with the interaction strength

$$V_{\mathbf{kk}'} = 2|V|^2 \frac{\varepsilon_{\mathbf{k}+\mathbf{k}'}}{\varepsilon_{\mathbf{k}+\mathbf{k}'}^2 - (E_{\mathbf{k}} - E_{\mathbf{k}'})^2}. \tag{6}$$

We define the gap function in the usual manner, $\Delta_{\mathbf{k}} = \sum_{\mathbf{k}'} V_{\mathbf{kk}'}\langle c_{-\mathbf{k}'\uparrow} c_{\mathbf{k}'\downarrow}\rangle$. The gap equation becomes

$$\Delta_{\mathbf{k}} = -\sum_{\mathbf{k}'} V_{\mathbf{kk}'} \frac{\Delta_{\mathbf{k}'}}{2\tilde{E}_{\mathbf{k}'}} \tanh\left(\frac{\tilde{E}_{\mathbf{k}'}}{2k_B T}\right), \tag{7}$$

where $\tilde{E}_{\mathbf{k}} = \sqrt{(E_{\mathbf{k}} - E_F)^2 + |\Delta_{\mathbf{k}}|^2}$ and E_F is the Fermi energy.

A. Quadratic magnon dispersion

In the continuum limit, we replace the discrete sum over momenta $\mathbf{k}$ with integrals over $E = E_{\mathbf{k}}$ and the angle φ, where $\mathbf{k} = k[\sin(\varphi),\cos(\varphi)]$. We assume that only the conduction electrons close to the Fermi surface form pairs. The magnon energy that appears in Eq. (6) is then given by $\varepsilon_{\mathbf{k}+\mathbf{k}'} \approx \varepsilon(\varphi',\varphi) = 4sJ\{2 - \cos(k_F a[\sin\varphi + \sin\varphi']) - \cos(k_F a[\cos\varphi + \cos\varphi'])\}$. Here, $k_F = \sqrt{2mE_F}/\hbar$ is the Fermi wave number. We assume that the NM is half filled, $k_F = \sqrt{2\pi}/a$. We introduce an energy scale $E^* = 4sJk_F^2a^2 = 8\pi sJ$ and scale all other energies with respect to E^*: $\delta = \Delta/E^*$, $\tau = k_BT/E^*$, $x = (E - E_F)/E^*$, $\tilde{x} = \tilde{E}/E^*$, and $\epsilon = \varepsilon/E^*$. In this way, the gap equation presented in Eq. (7) simplifies to

$$\delta(x,\varphi) = \frac{-\sqrt{2}\alpha}{\pi}\int_{-x_B}^{x_B} dx' \int_0^{2\pi} d\varphi' \times \frac{\epsilon(\varphi',\varphi)\delta(x',\varphi')}{\tilde{x}'[\epsilon^2(\varphi',\varphi) - (x-x')^2]} \tanh\left[\frac{\tilde{x}'}{2\tau}\right], \tag{8}$$

with the dimensionless coupling constant $\alpha = J_I^2/(16\sqrt{2}\pi E_F J) = J_I^2 ma^2/(16\sqrt{2}\pi^2\hbar^2 J)$. Here, the energy integral is restricted to the range $[E_F - x_B E^*, E_F + x_B E^*]$. We choose x_B—based on the value of α—such that all contributions to the gap from regions outside this range are vanishingly small. In the case $\alpha \ll 1$, the gap function has a narrow peak near $x = 0$, and therefore x_B can be much smaller than 1.

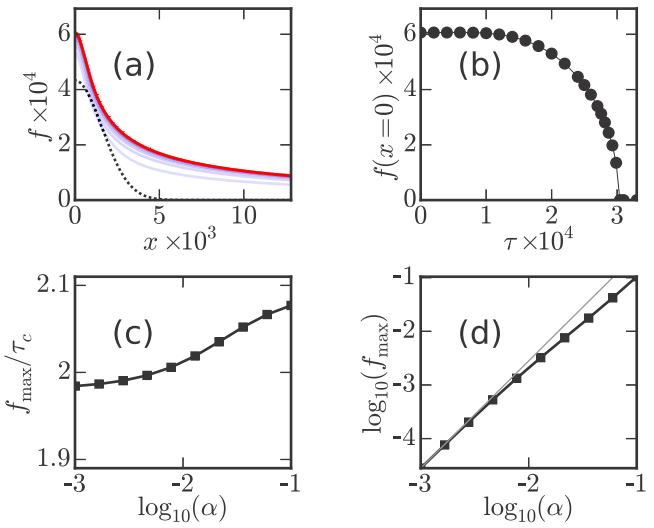

FIG. 2. Numerical solutions to the gap equation (9) determined through iteration. (a) Gaussian-shaped initial guess (dashed line) and the results of the first eight iterative calculations of the gap $f(x)$ (from light blue to red) when the dimensionless temperature is $\tau = 0$ and the coupling constant is $\alpha = 0.005$. Note that $f(-x) = f(x)$ and that the energy cutoff $x_B \approx 0.03$ lies outside the range of the plot. (b) Gap f at energy $x = 0$ as a function of τ for $\alpha = 0.005$. (c) Ratio between the maximum gap value $f_{\max}$ and the dimensionless critical temperature τ_c as a function of α. (d) α dependence of $f_{\max}$. The gray line corresponds to a quadratic dependence, $f_{\max} \sim \alpha^2$.

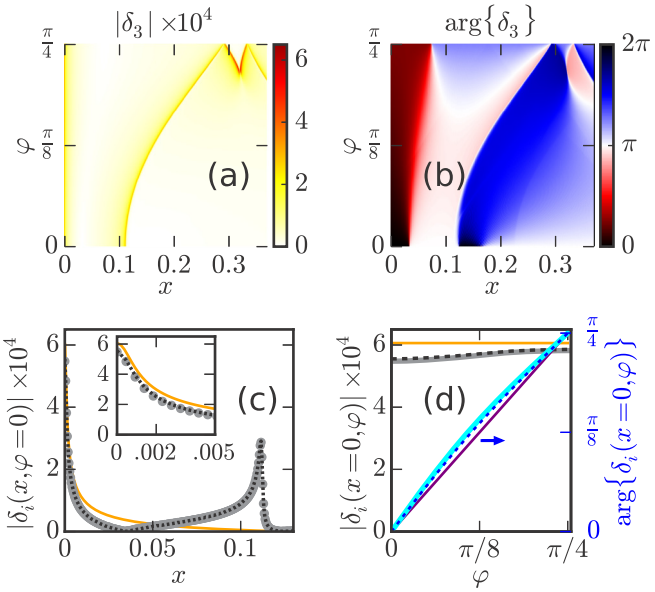

FIG. 3. Numerical iteration of the gap equation (8), starting from the solution to Eq. (9) as an initial guess, for $\tau = 0$ and $\alpha = 0.005$. (a), (b) Absolute value and phase of $\delta_3(x,\varphi)$, where the index 3 indicates the number of iterations. (c) $|\delta_i(x,\varphi=0)|$ for $i = 0$ (orange line), $i = 2$ (black dashed line), and $i = 3$ (gray circles). (d) $|\delta_i(x=0,\varphi)|$ (left axis) for $i = 0,2,3$, with the same colors as in (c), and the phase of $\delta_i(x=0,\varphi)$ (right axis) for $i = 0$ (purple), $i = 2$ (blue, dashed), and $i = 3$ (cyan, wide). Note that the difference from the second to third iteration is nearly indiscernible.

To gain a better understanding, we first consider a quadratic magnon dispersion, which matches that of Eq. (3) in the long-wavelength limit. Then, the dimensionless magnon energy becomes $\epsilon_q(\varphi',\varphi) = 1 + \cos(\varphi' - \varphi)$. Below, we check the correspondence between the solutions obtained using this dispersion and those obtained with the full magnon dispersion. For the quadratic magnon dispersion, the gap equation has a solution with p-wave symmetry, $\delta(x,\varphi) = f(x)\exp(\pm i\varphi)$. Applying this ansatz to Eq. (8), we calculate the integral over the angle φ' [38]. The gap equation becomes

$$f(x) = \alpha \int_{-x_B}^{x_B} dx'\, V(x-x') \frac{f(x') \tanh\left[\frac{\sqrt{x'^2+f(x')^2}}{2\tau}\right]}{\sqrt{x'^2+f(x')^2}}, \quad (9)$$

where $V(x-x') \approx 1/\sqrt{|x-x'|} - 2\sqrt{2}$. Conventional BCS theory replaces $V(x-x')$ by a constant with cutoffs in x and x', but we take the details of the effective interaction and the magnon dispersion into account.

Using a Gaussian centered at $x = 0$ as an initial guess, we solve Eq. (9) numerically through iteration [39]. Figure 2 shows the results. For a fixed coupling α, the maximum value occurs when $x = 0$ and $\tau = 0$. The dimensionless critical temperature τ_c is the temperature at which the gap vanishes. The gap equation can be solved analytically by approximating $V(x)$ as a constant with a cutoff. Then, $f_{\max}/\tau_c$ is approximately 1.76, which is slightly lower than what we find numerically; see Fig. 2(c).

B. Full magnon dispersion

We check that the solutions to Eq. (9), with the quadratic magnon dispersion, resemble the solutions to Eq. (8) for the full magnon dispersion. To this end, we iterate Eq. (8), starting from the solution to Eq. (9) [40]. We consider the zero-temperature case, $\tau = 0$. The symmetries $\delta(x,\varphi) = \delta(-x,\varphi) = i\delta(x,\varphi + \pi/2) = \delta^*(x,-\varphi)$, where δ^* is the complex conjugate of δ, imply that we need to consider only $x > 0$ and $0 < \varphi < \pi/4$. We show the results in Fig. 3. The third iteration of δ is shown in Figs. 3(a) and 3(b). After only three iterations, the differences between consecutive functions are already nearly imperceptible; see Figs. 3(c) and 3(d). For Eq. (9), the gap as a function of energy is peaked at the Fermi energy. The solutions to Eq. (8) exhibit a similarly shaped—but slightly lower and narrower—peak; see the inset of Fig. 3(c). Additional features of $\delta(x,\varphi)$ are at positions $[x,\varphi] = [\epsilon(\varphi',\varphi),\varphi]$ in the parameter space where the derivative of $\epsilon(\varphi',\varphi)$ with respect to φ' vanishes. In the following, we will use the quadratic magnon dispersion for further consideration, as we found only small modifications to the main peak of the gap function.

C. Influence of the Coulomb interaction

To estimate the extent to which the Coulomb interaction in the NM affects superconductivity, we add a screened Coulomb potential to our model. Therefore, we replace the potential $V_{\mathbf{k}\mathbf{k}'}$ by [41]

$$\tilde{V}_{\mathbf{k}\mathbf{k}'} = V_{\mathbf{k}\mathbf{k}'} + \frac{V_C}{N(\kappa + |\mathbf{k}-\mathbf{k}'|)} \quad (10)$$

in Eq. (5) and in the following equations. Here, $V_C = e^2/(2a^2\varepsilon_0)$, e is the elementary charge, ε_0 is the vacuum permittivity, and κ is the inverse screening length. As an estimate for the inverse screening length, we employ the result

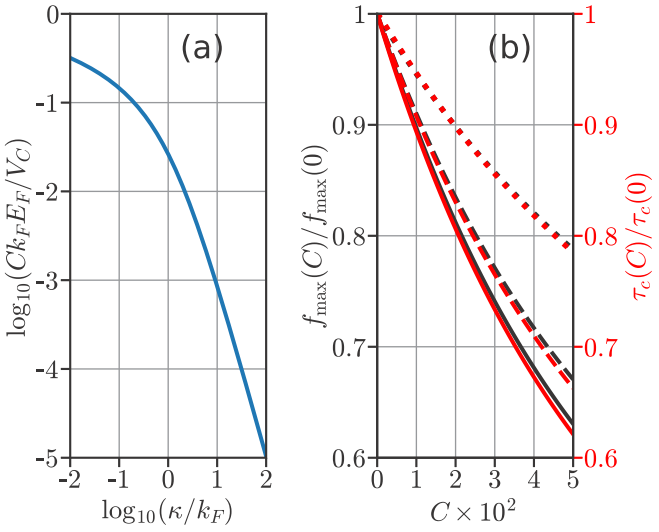

FIG. 4. The influence of the Coulomb interaction on the solutions of Eq. (9). (a) Dependence of the strength of the Coulomb interaction in the p-wave channel on the inverse screening length κ. (b) Dependence of the maximum value of the gap function $f_{\max}$ (black) and of the dimensionless critical temperature τ_c (red) on the Coulomb interaction strength C for the following values of α: 0.002 (solid lines), 0.008 (dashed), and 0.03 (dotted).

of the Lindhard theory in the static limit, $\kappa = m_e e^2/(2\pi\hbar^2\varepsilon_0)$, where m_e is the electron mass. We then find $\kappa \approx 3.8\,\text{Å}^{-1}$ and $V_C a^2 \approx 9.0 \times 10^{-9}$ eV m.

We express $|\mathbf{k}-\mathbf{k}'|$ as a function of φ and φ' using the approximation that $|\mathbf{k}| = |\mathbf{k}'| = k_F$. In this approximation, $|\mathbf{k}-\mathbf{k}'| = \sqrt{2}k_F\sqrt{1-\cos(\varphi-\varphi')}$. We account for the Coulomb interaction by replacing $V(x)$ with $\tilde{V}(x) = V(x) - C/\alpha$ in Eq. (9), where C is given by

$$C = \frac{V_C}{8\sqrt{2}\pi k_F E_F}\int_{-\pi}^{\pi} d\tilde{\varphi}\,\frac{\cos(\tilde{\varphi})}{\frac{\kappa}{\sqrt{2}k_F} + \sqrt{1-\cos(\tilde{\varphi})}}. \tag{11}$$

The integral in Eq. (11) can be evaluated analytically [42].

We illustrate the dependence of the constant C on the inverse screening length κ in Fig. 4(a). We determine how the gap and the critical temperature depend on the value of C by solving the modified version of Eq. (9). We use the same iterative method to solve the gap equation as before. The results are presented in Fig. 4(b).

IV. ESTIMATING PARAMETERS

Next, we estimate the critical temperatures T_c for two possible experimental realizations: one with yttrium iron garnet (YIG) as the FI and one with europium oxide (EuO). The NM layer is gold in both cases. We use different procedures for YIG and EuO when we estimate the interface coupling J_I. For YIG, we estimate J_I based on the spin-mixing conductance, whereas for EuO, we use measurements of an effective Zeeman field. For the FIs, we assume—encouraged by the results presented in Fig. 3—that the low-energy magnons dominate the gap. The relevant magnons are therefore well described by the quadratic dispersion.

A. YIG-Au-YIG trilayer

Our model assumes the same lattice structure throughout the YIG-Au-YIG trilayer. However, in reality, the unit cell of YIG is much larger than that of Au. To capture the properties of YIG in our model, we fit the parameters such that the FIs have the same exchange stiffness ($D/k_B = 71$ K nm^2 [43]) and saturation magnetization ($M_s = 1.6 \times 10^5$ A/m [43]) as those of bulk YIG. We assume that each YIG layer has a thickness equal to the bulk lattice constant of YIG ($a_{\text{YIG}} \approx 12$ Å [43]). We use the thickness, the saturation magnetization, and the electron gyromagnetic ratio γ_e to estimate the spin quantum number $s = M_s a_{\text{YIG}} a^2/(\hbar\gamma_e)$. We determine the exchange interaction $J = D/(2a^2 s)$ using the quadratic dispersion approximation. The lattice spacing a remains undetermined.

In the bulk, gold has an fcc lattice and a half-filled conduction band. We use experimental values of the Fermi energy ($E_F^{\text{B}} = 5.5$ eV [44]) and the Sharvin conductance ($g_{\text{Sh}} = 12$ nm^{-2} [6]) to determine the effective mass, $m_{\text{Au}} = 2\pi g_{\text{Sh}}\hbar^2/E_F^{\text{B}}$, of bulk gold. We assume that the monolayer is half filled and has an effective electron mass m_{Au}. Below, we will define a simple cubic tight-binding model for bulk gold. The lattice constant of that model a_{t} is approximately 20% smaller than the bulk nearest-neighbor distance of actual gold. We consider the case where the trilayer lattice constant a is equal to a_{t}. We choose the lattice constant in this way because it simplifies our estimate for J_I. The effective mass and the lattice constant in a physical realization might be slightly different, but the agreement should be sufficient to estimate T_c to an order of magnitude.

We now define a model for a YIG-Au bilayer using the same interface exchange Hamiltonian—H_{int} of Eq. (2)—as in the trilayer. We use a simple cubic lattice for the gold and a square lattice for the YIG. We assume that the lattices of YIG and Au are matched at the interface in the same way as in the trilayer. Then, the lattice structure at the interface is the same in both models. We therefore assume that the interfacial exchange coupling J_I of the trilayer is the same as in the bilayer. We estimate J_I based on measurements of the spin-mixing conductance in YIG-Au bilayers [45–47]. Extrinsic effects related to the quality of the interface can influence the electron-magnon coupling. We account for such effects because we scale J_I according to electron-magnon transport measurements.

We use the same model for the YIG in the bilayer as for the trilayer; however, for the gold, we employ a tight-binding model of the form $H_{\text{t}} = -t_{\text{t}}\sum_\sigma\sum_i\sum_{j\in\text{NN}(i)} c_{i\sigma}^\dagger c_{j\sigma}$. The Hamiltonian of the bilayer is $H_{\text{B}} = H_{\text{t}} + H_{\text{FI}}^A + H_{\text{int}}$. We disregard the proximity-induced Zeeman field in the bilayer. The energy eigenstates $c_{\mathbf{q}\sigma}^{\text{t}}$ and the dispersion $E_{\mathbf{q}}^{\text{t}} = 4t_{\text{t}}[3 - \cos(q_x a_{\text{t}}) - \cos(q_y a_{\text{t}}) - \cos(q_z a_{\text{t}})]$ of H_{t} are well known. Under the assumption of half filling, we find that $t_{\text{t}} = E_F^{\text{B}}/12$ and $a_{\text{t}} = \sqrt{0.63/g_{\text{Sh}}}$. We use the same experimental values for E_F^{B} and g_{Sh} [6,44] as before.

To first order in the bosonic operators, $H_{\text{int}} = \sum_{\mathbf{kq}} V_{\text{t}} a_{\mathbf{k}} c_{\mathbf{q}+\mathbf{k},\downarrow}^{\text{t}\dagger} c_{\mathbf{q}\uparrow}^{\text{t}}$. The coupling strength V_{t} is proportional to the amplitudes of the tight-binding-model eigenstates at the interface, $V_{\text{t}} = 2V\sin(q_x a_{\text{t}})\sin([k_x + q_x]a_{\text{t}})$. The spin-mixing conductance can now be calculated for the ferromagnetic resonance (FMR) mode, resulting [37] in

$g_{\uparrow\downarrow} = 4a_t^2 V_0 s N/(2\pi)^2$, where

$$V_0 = \iint |V|^2 \sin(q_x a_t)^2 \sin(q_x' a_t)^2 \delta(q_y - q_y') \times \delta(q_z - q_z')\delta\left(E_{\mathbf{q}}^t - E_F\right)\delta\left(E_{\mathbf{q}'}^t - E_F\right) d^3\mathbf{q} d^3\mathbf{q}'. \quad (12)$$

We evaluate V_0 numerically and use it to estimate the interfacial exchange coupling $J_I = 0.33 \times 2\pi t_t a_t \sqrt{g_{\uparrow\downarrow}}/s$. Using $E^* = 8\pi s J$, we find that E^* is approximately 1.5 eV. We find the coupling constant α from the relation $\alpha = J_I^2 m a^2/(16\sqrt{2}\pi^2\hbar^2 J)$. The reported experimental values for the spin-mixing conductance range from 1.2 to 6 nm^{-2} [45–47]. In turn, this implies that α lies in the range of 0.0014–0.007. The corresponding critical temperatures range from 0.5 to 10 K.

B. EuO-Au-EuO trilayer

Next, we consider a EuO-Au-EuO trilayer. EuO has an fcc lattice structure with a lattice constant of 5.1 Å, a spin quantum number of $s = 7/2$, and a nearest-neighbor exchange coupling of $J/k_B = 0.6$ K [48]. The nodes on a (100) surface of an fcc lattice form a square lattice, in which the lattice constant equals the bulk nearest-neighbor distance. We assume that the monolayer has the same structure, and therefore set a equal to the distance between nearest neighbors in bulk EuO. We use the same effective mass m_{Au} as for the YIG-Au-YIG trilayer. Then, the Fermi energy E_F is 1.8 eV, and the energy scale E^*/k_B is approximately 53 K. Values on the order of 10 meV have been reported for the interfacial exchange coupling strengths J_I [49] in EuO/Al [7], EuO/V [8], and EuS/Al [9,10]. These estimates were based on measurements of a proximity-induced effective Zeeman field. Under the assumption that J_I is in the range of 5–15 meV, we find a wide range of values (0.004–0.03) for α. We estimate the corresponding critical temperatures T_c numerically, giving the range 0.01–0.4 K.

C. Coulomb interaction

We estimate the impact of the Coulomb interaction for the YIG-Au-YIG and EuO-Au-EuO trilayers using the parameters from Secs. IV A and IV B and the screened Coulomb potential from Sec. III C. For the constant C of Eq. (11), we find the values 1.3×10^{-2} (YIG-Au-YIG) and 9.4×10^{-3} (EuO-Au-EuO). We see from Fig. 4(b) that the maximum value of the gap function and the critical temperature both decrease by approximately 10% when we include the screened Coulomb potential. Therefore, the Coulomb interaction does not affect our order-of-magnitude estimates for the critical temperature.

D. Normal metals with multiple atomic layers

As an estimate for thicker NM layers, one can scale the electron-magnon coupling in Eq. (4) by $V \to Va/d$, where d is the thickness of the NM. In this approximation, the critical temperature scales as $T_c \sim d^{-4}$ (for $\alpha \ll 1$) and remains experimentally accessible if the NM is a few atomic layers thick.

V. CONCLUSIONS

In conclusion, interfacial coupling to magnons induces p-wave superconductivity in metals. Our calculated critical temperatures are experimentally accessible. The gap size strongly depends on the magnitude of the interfacial exchange coupling. The thickness dependence, the robustness against disorder, and potential influence by the magnon self-energy and renormalization effects should be explored in the future.

ACKNOWLEDGMENTS

We thank W. Belzig for useful discussions. This work was partially supported by the European Research Council via Advanced Grant No. 669442 "Insulatronics" and the Research Council of Norway through its Centres of Excellence funding scheme, Project No. 262633, "QuSpin."

[1] P. Bruno, Phys. Rev. B **52**, 411 (1995).
[2] Y. Tserkovnyak, A. Brataas, and G. E. W. Bauer, Phys. Rev. Lett. **88**, 117601 (2002).
[3] T. Tokuyasu, J. A. Sauls, and D. Rainer, Phys. Rev. B **38**, 8823 (1988).
[4] S. M. Rezende, R. L. Rodríguez-Suárez, and A. Azevedo, Phys. Rev. B **88**, 014404 (2013).
[5] Y. Kajiwara, K. Harii, S. Takahashi, J. Ohe, K. Uchida, M. Mizuguchi, H. Umezawa, H. Kawai, K. Ando, K. Takanash, S. Maekawa, and E. Saitoh, Nature (London) **464**, 7286 (2010).
[6] Y. Tserkovnyak, A. Brataas, G. E. W. Bauer, and B. I. Halperin, Rev. Mod. Phys. **77**, 1375 (2005).
[7] J. E. Tkaczyk, Ph.D. thesis, MIT, 1988.
[8] G. M. Roesler, M. E. Filipkowski, P. R. Broussard, Y. U. Idzerda, M. S. Osofsky, and R. J. Soulen, Proc. SPIE **2157**, 285 (1994).
[9] X. Hao, J. S. Moodera, and R. Meservey, Phys. Rev. Lett. **67**, 1342 (1991).
[10] G.-X. Miao, J. Chang, B. A. Assaf, D. Heiman, and J. S. Moodera, Nat. Commun. **5**, 3682 (2014).
[11] K. Ando, S. Takahashi, J. Ieda, Y. Kajiwara, H. Nakayama, T. Yoshino, K. Harii, Y. Fujikawa, M. Matsuo, S. Maekawa, and E. Saitoh, J. Appl. Phys. **109**, 103913 (2010).
[12] M. B. Jungfleisch, A. V. Chumak, A. Kehlberger, V. Lauer, D. H. Kim, M. C. Onbasli, C. A. Ross, M. Kläui, and B. Hillebrands, Phys. Rev. B **91**, 134407 (2015).
[13] L. J. Cornelissen, J. Liu, R. A. Duine, J. B. Youssef, and B. J. van Wees, Nat. Phys. **11**, 12 (2015).
[14] C. O. Avci, A. Quindeau, C. Pai, M. Mann, L. Caretta, A. S. Tang, M. C. Onbasli, C. A. Ross, and G. S. D. Beach, Nat. Mater. **16**, 4812 (2016).
[15] A. A. Serga, A. V. Chumak, and B. Hillebrands, J. Phys. D. **43**, 264002 (2010).
[16] T. R. Kirkpatrick and D. Belitz, Phys. Rev. B **67**, 024515 (2003).
[17] N. Karchev, Phys. Rev. B **67**, 054416 (2003).
[18] S. S. Saxena, P. Agarwal, K. Ahilan, F. M. Grosche, R. K. W. Haselwimmer, M. J. Steiner, E. Pugh, I. R. Walker, S. Julian, P. Monthoux, G. G. Lonzarich, A. H. I. Sheikin, D. Braithwaite, and J. Flouquet, Nature (London) **406**, 6796 (2000).

[19] D. Aoki, A. Huxley, E. Ressouche, D. Braithwaite, J. Flouquet, J. Brison, E. Lhotel, and C. Paulsen, Nature (London) **413**, 6856 (2001).
[20] C. Pfleiderer, M. Uhlarz, S. M. Hayden, R. Vollmer, H. v. Löhneysen, N. R. Bernhoeft, and G. G. Lonzarich, Nature (London) **412**, 6842 (2001).
[21] D. Fay and J. Appel, Phys. Rev. B **22**, 3173 (1980).
[22] N. Karchev, Europhys. Lett. **110**, 27004 (2015).
[23] Y. Saito, T. Nojima, and Y. Iwasa, Nat. Rev. Mater. **2**, 16094 (2016).
[24] S. Gariglio, M. Gabay, J. Mannhart, and J.-M. Triscone, Physica C **514**, 189 (2015).
[25] N. Reyren, S. Thiel, A. D. Caviglia, L. F. Kourkoutis, G. Hammerl, C. Richter, C. W. Schneider, T. Kopp, A.-S. Rüetschi, D. Jaccard, M. Gabay, D. A. Muller, J.-M. Triscone, and J. Mannhart, Science **317**, 1196 (2007).
[26] Q. Y. Wang, Z. Li, W. H. Zhang, Z. C. Zhang, J. S. Zhang, W. Li, H. Ding, Y. B. Ou, P. Deng, K. Chang, J. Wen, C. L. Song, K. He, J. F. Jia, S. H. Ji, Y. Y. Wang, L. L. Wang, X. Chen, X. C. Ma, and Q. K. Xue, Chin. Phys. Lett. **29**, 037402 (2012).
[27] H. Boschker, C. Richter, E. Fillis-Tsirakis, C. W. Schneider, and J. Mannhart, Sci. Rep. **5**, 12309 (2015).
[28] S. N. Klimin, J. Tempere, J. T. Devreese, and D. van der Marel, Phys. Rev. B **89**, 184514 (2014).
[29] B. Li, Z. W. Xing, G. Q. Huang, and D. Y. Xing, J. Appl. Phys. **115**, 193907 (2014).
[30] X.-X. Gong, H.-X. Zhou, P.-C. Xu, D. Yue, K. Zhu, X.-F. Jin, H. Tian, G.-J. Zhao, and T.-Y. Chen, Chin. Phys. Lett. **32**, 067402 (2015).
[31] C. Stephanos, T. Kopp, J. Mannhart, and P. J. Hirschfeld, Phys. Rev. B **84**, 100510(R) (2011).
[32] D. Allender, J. Bray, and J. Bardeen, Phys. Rev. B **7**, 1020 (1973).
[33] V. Koerting, Q. Yuan, P. J. Hirschfeld, T. Kopp, and J. Mannhart, Phys. Rev. B **71**, 104510 (2005).
[34] X. Gong, M. Kargarian, A. Stern, D. Yue, H. Zhou, X. Jin, V. M. Galitski, V. M. Yakovenko, and J. Xia, Sci. Adv. **3**, e1602579 (2017).
[35] M. Kargarian, D. K. Efimkin, and V. Galitski, Phys. Rev. Lett. **117**, 076806 (2016).
[36] S. Takahashi, E. Saitoh, and S. Maekawa, J. Phys.: Conf. Ser. **200**, 062030 (2010).
[37] S. A. Bender, R. A. Duine, and Y. Tserkovnyak, Phys. Rev. Lett. **108**, 246601 (2012).
[38] For the integration, we use the Cauchy principle value and the fact that $\Delta x = |x - x'| \ll 1$,

$$V(\Delta x) = -\frac{\sqrt{2}}{\pi}\int_0^{2\pi} d\tilde{\varphi}\,\frac{(1+\cos\tilde{\varphi})\cos\tilde{\varphi}}{(1+\cos\tilde{\varphi})^2 - \Delta x^2}$$
$$= \frac{1+|\Delta x|}{\sqrt{\Delta x^2/2 + \Delta x}} - 2\sqrt{2} \approx \frac{1}{\sqrt{\Delta x}} - 2\sqrt{2}.$$

[39] To eliminate the singularity in $V(x-x')$ at $x' = x$ for the numerical integration, we replace $V(x-x')$ in Eq. (9) with $\int_0^x d\tilde{x}\,V(\tilde{x}-x')$ and $f(x)$ on the left-hand side of Eq. (9) with $F(x) = \int_0^x d\tilde{x}\,f(\tilde{x})$. In each iteration, we numerically evaluate the integral over x' in the resulting equation and obtain $f(x)$ by numerically differentiating F.
[40] We eliminate singularities from the integral over x' in Eq. (8) by replacing the factor $U(\varphi',\varphi,x',x) = 1/[\epsilon^2(\varphi',\varphi) - (x-x')^2]$ in the integrand with $\int_0^x d\tilde{X}\int_0^{\tilde{X}} d\tilde{x}\,U(\varphi',\varphi,x',\tilde{x})$ and $\delta(x,\varphi)$ with $D(x,\varphi) = \int_0^x d\tilde{X}\int_0^{\tilde{X}} d\tilde{x}\,\delta(\tilde{x},\varphi)$. In each iteration, we find D by numerically integrating over x' and then find δ by numerically differentiating D twice.
[41] T. Ando, A. B. Fowler, and F. Stern, Rev. Mod. Phys. **54**, 437 (1982).
[42] We want to calculate the integral $A(\kappa/[\sqrt{2}k_F])$, where

$$A(c) := \int_{-\pi}^{\pi} d\tilde{\varphi}\,\frac{\cos(\tilde{\varphi})}{c + \sqrt{1-\cos(\tilde{\varphi})}}$$
$$= 4\left[c\frac{\pi}{2} - \sqrt{2} + \frac{1-c^2}{\sqrt{2}}\underbrace{\int_0^{\pi/2} d\theta\,\frac{1}{\sin\theta + \tilde{c}}}_{=:B(\tilde{c})}\right].$$

Here, we have defined $\tilde{c} = c/\sqrt{2} = \kappa/(2k_F)$. The integral $B(\tilde{c})$ can be solved analytically, giving

$$B(\tilde{c}) = \begin{cases} 1 & \text{if } \tilde{c} = 1, \\ \frac{2}{\sqrt{\tilde{c}^2-1}}\arctan\left(\frac{\tilde{c}-1}{\sqrt{\tilde{c}^2-1}}\right) & \text{if } \tilde{c} > 1, \\ \frac{1}{\sqrt{1-\tilde{c}^2}}\ln\left(\frac{\tilde{c}}{1-\sqrt{1-\tilde{c}^2}}\right) & \text{if } \tilde{c} < 1. \end{cases}$$

[43] S. Klingler, A. V. Chumak, T. Mewes, B. Khodadadi, C. Mewes, C. Dubs, O. Surzhenko, B. Hillebrands, and A. Conca, J. Phys. D **48**, 015001 (2015).
[44] N. W. Ashcroft and N. D. Mermin, *Solid State Physics* (Holt, Rinehart and Winston, New York, 1976).
[45] B. Heinrich, C. Burrowes, E. Montoya, B. Kardasz, E. Girt, Y. Y. Song, Y. Sun, and M. Wu, Phys. Rev. Lett. **107**, 066604 (2011).
[46] C. Burrowes, B. Heinrich, B. Kardasz, E. Montoya, E. Girt, Y. Sun, Y. Song, and M. Wu, Appl. Phys. Lett. **100**, 092403 (2012).
[47] M. Haertinger, C. H. Back, J. Lotze, M. Weiler, S. Geprägs, H. Huebl, S. T. B. Goennenwein, and G. Woltersdorf, Phys. Rev. B **92**, 054437 (2015).
[48] A. Mauger and C. Godart, Phys. Rep. **141**, 51 (1986).
[49] Note that the strength of the exchange coupling is defined differently in Refs. [7,8]; the values reported there must be divided by 2 to obtain the value of J_1 as it is defined in this article.